JCTC Journal of Chemical Theory and Computation

Article

pubs.acs.org/JCTC

Geometries and Vertical Excitation Energies in Retinal Analogues Resolved at the CASPT2 Level of Theory: Critical Assessment of the Performance of CASSCF, CC2, and DFT Methods

Elżbieta Walczak,[†] Borys Szefczyk,[†] and Tadeusz Andruniów*

Wroclaw University of Technology, Institute of Physical & Theoretical Chemistry, Wyb. Wyspianskiego 27, 50-370 Wroclaw, Poland

Supporting Information

ABSTRACT: A systematic investigation of structural properties and vertical excitation energies of a series of structurally modified *11-cis-retinal* chromophores in vacuo was performed by means of multiconfigurational second-order perturbation theory (CASPT2). CASPT2-based geometries agree reasonably well with Møller−Plesset second-order perturbation theory (MP2), local second-order approximate coupled cluster singles and doubles (LCC2), and density functional theory (DFT) geometries, while the complete active space self-consistent field (CASSCF) method exaggerates dramatically the bond length pattern in the polyene chain. The quality of the resulting vertical excitation energies obtained by employing CASSCF, second-order approximate coupled cluster singles and doubles (CC2), LCC2, and time-dependent density functional theory (TD-DFT) approaches is assessed with respect to the CASPT2 data. We show that the commonly used CASSCF/CASPT2 approach works reasonably well in the case of vertical excitation energies of planar structures, but lack of dynamic correlation leads to large errors in energetics for strongly strained structures. For example, the highly twisted conformers of *9,10-dimethyl* and *9,10,13-trimethyl* species are found as global minima at the CASSCF level, whereas they turn almost planar at the CASPT2, MP2, LCC2, and DFT levels of theory. The CC2 method has shown a remarkable performance, manifested by a maximum deviation of 0.05 eV from the reference CASPT2 results, whereas the local version of CC2 seems to fail to describe the charge-transfer character of the $S_0 \rightarrow S_1$ transitions correctly. We believe that our CASPT2 benchmark set will provide a reference that can be utilized for validation and development studies on *11-cis-retinal* protonated Schiff base chromophore analogues.

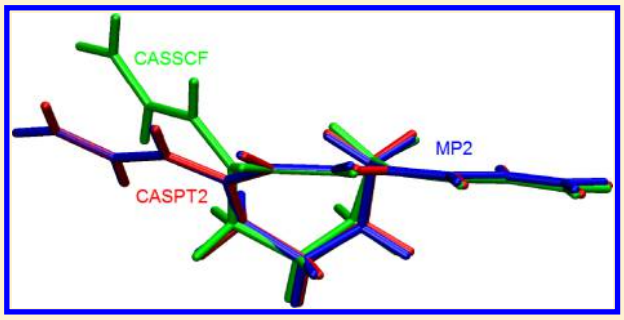

1. INTODUCTION

The light-transducing pigment rhodopsin is the photosensor in the vertebrate retina responsible for scotopic vision. Rhodopsin contains an *11-cis-retinal* chromophore attached to the ε-amino group of the Lys296 residue of the apoprotein opsin through a protonated Schiff base linkage. The primary photochemical event in rhodopsin, after absorption of a photon, is the *11-cis* to *all-trans* isomerization of the retinal chromophore that, in turn, triggers a series of protein conformational changes. The photoreaction is highly stereoselective in the protein cavity, and the primary photoproduct—photorhodopsin—is formed in only 200−250 fs,[1] making it one of the fastest and most efficient (quantum yield is 0.65[2]) reactions known to date. Within 5 ps, photorhodopsin thermally relaxes to bathorhodopsin containing a distorted *all-trans* retinal.[3] The absorbed photon energy stored in bathorhodopsin, 35 kcal/mol,[4] is used to drive the conformational changes of the protein.

Retinal analogues probed in a protein environment have been the subject of extensive experimental[5−9] and computational effort.[10−12] It has been demonstrated that the retinal binding cavity is flexible enough to accommodate structurally modified retinals to form pigment analogues. However, significant changes in the excited-state lifetime and efficiency of the photoisomerization process have been observed for artificial rhodopsins where the native *11-cis-retinal* chromophore was modified through addition or deletion of methyl groups along the polyene chain of retinal.[13−19] An ultrafast kinetics of the isomerization process and high quantum yield are often attributed to nonbonded interactions between the methyl group at C13 and hydrogen at C10, causing a torsional distortion of the central part of the chromophore chain.[15] Therefore, the central question of many studies was the impact of 13- and 9-methyl groups by using 13-demethyl and 9-demethyl retinal analogues and of an additional methyl group at C10 by using 10-methyl and 10-methyl-13-demethyl retinal analogues on receptor activation.[13−19] To gain insight into the photointermediates' structures and absorption properties, Kandori and his co-workers have investigated pigment containing retinal analogues with a locked C11−C12 bond by five-, seven-, and eight-membered rings using picosecond absorption[20,21] and femtosecond fluorescence[22] spectroscopy. These results suggested that the flexibility of the central double

Received: May 23, 2013
Published: September 27, 2013

bond is essential to the primary process in rhodopsin.[21] In fact, the photoisomerization process in rhodopsin with locked-11.5 chromophore was found to be prohibited.

Most of these analogues and their models have been thoroughly investigated in vacuo using quantum chemistry methodology. Olivucci and co-workers,[23,24] on the basis of CASSCF/CASPT2 calculations, demonstrated the possibility of tuning the excited-state lifetime by incorporating a specific lock (five-, seven-, or eight-membered ring) within the RPSB (retinal protonated Schiff base) polyene chain. Send and Sundholm[25] reported the characteristic features of Franck−Condon (FC) relaxation in native and locked-11.5 retinal chromophores in terms of TD-DFT. A broad spectrum of ab initio methods was employed in the study by Valsson, Angeli, and Filippi to obtain excitation energies of different structural models of RPSB.[26,27] Valsson and Filippi have also shown the importance of a balanced description of static and dynamic correlation in the investigation of the excited-state relaxation process in retinal models.[26] CASSCF excited-state molecular dynamics simulations for four-double-bond retinal models with different methyl substitution patterns at C10 and C13 resulted in a conclusion that a chemical substitution in the polyene chain and the corresponding geometric distortion may determine the outcome of the isomerization.[10]

MP2 and coupled-cluster are regarded as reliable methods to investigate molecular structures of retinals in their ground electronic states since the wave function describing the ground-state equilibrium structure is single-configurational; as we will explain below, CASPT2 and MP2 geometries (in the same basis set) are essentially identical. However, multireference methods with a balanced description of static and dynamic electron correlation effects need to be considered when studying ground-state geometries and energies near the conical intersection region. Because the molecular size of retinals precludes the usage of highly accurate multireference ab initio methods, for example, multireference configuration interaction (MRCI), CASPT2 can be a method of choice not only for generation of excitation energies but also for molecular structure optimization in both the ground and the excited states. In our view, there is a need to characterize molecular structures of retinal models at the CASPT2 level of theory since the use of CASPT2 was confined to minimal retinal three-double-bond (PSB3)[26,28−30] and four-double-bond (PSB4)[26] models. An absence of analytic gradients together with the high computational cost makes it impossible to use the CASPT2 method with extensive basis sets during geometry optimization procedures. For this reason, we aim at assessing the significance of basis set effects on the ground-state molecular structures of retinal models.

Here, we use the CASPT2 approach to optimize the geometries and calculate vertical excitation energies in vacuo for a five-double-bond model PSB5 of RPSB. In particular, we look at two kinds of RPSB analogues: (a) with methylated and/or demethylated retinal backbones and (b) with a locked C11−C12 bond by five-, seven-, and eight-membered rings (see Figure 1). To the best of our knowledge, this is the first systematic CASPT2 study on both geometries and vertical excitation energies in PSB5 (including five double bonds) models; therefore, it may provide the reference data required to assess the accuracy of the results produced by lower-level methods, for example, DFT, CASSCF, or approximate coupled cluster (CC2 and LCC2).

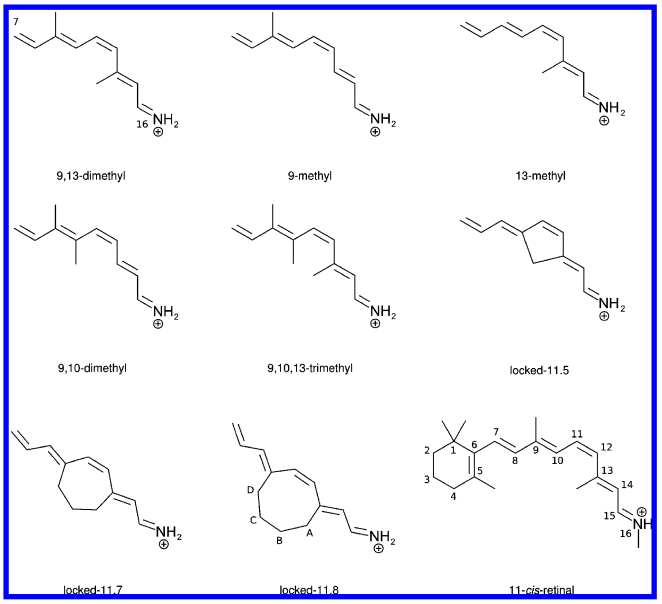

Figure 1. Model RPSB chromophores investigated in this study. The atom numbering for full RPSB is used for all investigated models.

2. METHODS

2.1. Models. All calculations have been performed for RPSB models shown in Figure 1. *9,13-Dimethyl* is a model corresponding to the native RPSB, whereas *9,10-dimethyl, 9-methyl, 13-methyl*, and *9,10,13-trimethyl* are various methylated and demethylated variants. However, these models do not include the β-ionone ring. In all cases, except for *9,10-dimethyl* and *9,10,13-trimethyl*, S_0 equilibrium structures were planar, although the symmetry was not imposed during geometry optimizations. These two models have methyl groups attached to neighboring atoms, and therefore, a significant sterical hindrance may disturb the planarity of the molecule. In these two cases, a planar (C_s) and twisted (*twist*) structures were investigated. In addition to the methylated and demethylated models, three systems were studied, in which the C11−C12 bond rotation is limited by a five- (*locked-11.5*), seven- (*locked-11.7*), and eight-membered ring (*locked-11.8*). The latter one has three ground-state minima that were investigated: the chairlike (*locked-11.8*) and two pseudoboat conformations (*locked-11.8-b1* and *locked-11.8-b2*).

2.2. Geometry Optimization and Vertical Excitations. Ground-state geometry optimization for retinal analogues at CASSCF and CASPT2 levels of theory using 6-31G(d) and atomic natural orbital (ANO-L-VDZP)[31] basis sets (except for CASSCF/ANO-L-VDZP) were done using Molpro[32] quantum chemistry package. The CASPT2 calculations utilized the RS2C program.[33] The Molcas package was used in CASSCF/ANO-L-VDZP geometry optimization and for calculations of properties at the CASPT2 level of theory.

In most cases, the calculations have been initialized with the geometries found in the literature, as some of the systems have been studied already.[23,24,34−36] In other cases, a reasonable initial geometry has been prepared in the Molden program.[37] The active space used in CASSCF and CASPT2 was 10 orbitals and 10 electrons, comprising the whole π-orbital system. The energy minima were found using the single-root CASSCF wave function in both CASSCF and CASPT2 geometry optimization procedures.

Table 1. Bond Length Alternation (BLA; in Å) of the Ground-State Equilibrium Structure of the Retinyl Chain of RPSB Models. Mean, Maximum, and Minimum Absolute Errors Are Also Given (in Å)

	CASSCF		CASPT2[a]		MP2	LCC2	BLYP	B3LYP	CAM-B3LYP
model	6-31G(d)	ANO[b]	6-31G(d)	ANO[b]			cc-pVTZ		
9,13-dimethyl	0.101	0.101	0.050	0.042	0.053	0.055	0.042	0.049	0.061
9-methyl	0.097	0.097	0.047	0.045	0.052	0.051	0.039	0.046	0.058
13-methyl	0.100	0.100	0.052	0.045	0.056	0.056	0.044	0.051	0.064
9,10-dimethyl (*twist*)	0.117	0.117	0.050	0.035	0.051	0.052	0.039	0.047	0.059
9,10-dimethyl (C_s)	0.100	0.099	0.046	0.038	0.049	0.052	0.039	0.046	0.057
9,10,13-trimethyl (*twist*)	0.122	0.121	0.091	0.042	0.054	0.057	0.042	0.050	0.066
9,10,13-trimethyl (C_s)	0.104	0.104	0.050	0.041	0.051	0.054	0.040	0.048	0.062
locked-11.5	0.099	0.099	0.051	0.044	0.054	0.053	0.047	0.054	0.066
locked-11.7	0.098	0.097	0.045	0.038	0.050	0.051	0.040	0.048	0.060
locked-11.8	0.113	0.112	0.057	0.046	0.055	0.057	0.045	0.053	0.068
locked-11.8-b1	0.117	0.117	0.051	0.040	0.052	0.054	0.042	0.050	0.063
locked-11.8-b2	0.117	0.116	0.052	0.039	0.051	0.053	0.041	0.049	0.062
mean absolute error	0.055	0.054	0.006	0.011		0.002	0.011	0.003	0.010
max absolute error	0.068	0.067	0.037	0.016		0.003	0.012	0.005	0.012
min absolute error	0.044	0.044	0.001	0.007		0.000	0.007	0.000	0.006

[a]BLA and absolute error for *locked-11.5* in the cc-pVTZ basis set is 0.049 and 0.005 Å, respectively. [b]ANO stands for the ANO-L-VDZP basis set.

The excitation energies at CASSCF and CASPT2 levels were calculated at the FC point, which means that only vertical excitations from the ground-state minimum were considered. The wave function was constructed from S_0 and S_1 roots with equal weights. In the CASPT2 calculations, an empirical IPEA-shift parameter has been recently introduced in the Hamiltonian.[38] Therefore, we either use a standard value of this parameter, which is 0.25, or we set the parameter to zero; that is, it is not used. CASPT2 calculations were based on both single-state (SS) and multistate (MS)[39] schemes. If needed, an additional level shift (0.1 au) to the Hamiltonian[40] was added. Unless indicated, CASPT2 excitation energies were obtained using the SS-CASPT2 formalism with the standard IPEA-shift parameter (S-IPEA).

The LCC2, *local* CC2 method, is a cheaper variant of the coupled cluster method, additionally making use of orbital localization. The approximation is based on restricting the dynamic correlation to pairs and triplets of localized orbitals.[41] The implementation of the method in Molpro uses the density fitting approximation,[42] which replaces the one-electron density elements in Coulomb integrals with auxiliary basis functions; we use the cc-pVTZ basis set for both geometry optimization and excitation energy calculations. In this way, two-electron, four-index integrals are replaced with two-electron integrals with two and three indices. In LCC2 calculations, the excitations to S_1 and S_2 were included, but the properties were computed only for S_0 and S_1.

MP2 geometry optimization and the coupled-cluster approximate singles and doubles (CC2) vertical excitation calculations for three states were performed using the resolution-of-the-identity (RI) scheme[43] with the auxiliary basis set for Dunning's cc-pVTZ basis set[44] within the Turbomole package.[45] Gaussian 09[46] was used in searching for equilibrium structures employing the DFT method along with BLYP,[47,48] B3LYP,[49,50] CAM-B3LYP,[51] and PBE0[52] functionals. Subsequently, vertical excitation energies for 10 states were computed using the TD-DFT approach.

Additionally, to investigate the impact of various geometries on the $S_0 \rightarrow S_1$ excitation energies, the CASPT2/ANO-L-VDZP energy evaluation for all MP2- and DFT-based geometries was carried out in the Molcas[53] program. For the CASPT2 method, we use the same setup as described above. The default convergence criteria for geometry optimization and energy evaluation were used for all quantum chemistry software.

Properties, such as oscillator strengths or change in electric dipole moments upon electron excitation, were obtained at CASSCF and CASPT2 using Molcas,[53] at LCC2 using Molpro software,[32] at CC2 using Turbomole,[45] and finally at TD-DFT using the Gaussian[46] suite of programs.

3. RESULTS AND DISCUSSION

The geometry of *11-cis-retinal* protonated Schiff base chromophore models shown in Figure 1 has been optimized using multireference CASSCF and CASPT2, as well as single-reference MP2 and coupled clusters LCC2 methods. Also, the performance of DFT's gradient-corrected and hybrid functionals was tested against the CASPT2 and MP2 methods. The results of a geometry optimization of the analogues' structures, presented in Table 1 and Figure 2, are analyzed in terms of CC and CN bond distances, and bond length alternation (BLA) values (BLA is defined as the difference between the averages of the double and single bond distances along C7···N conjugated chain). Mean, maximum, and minimum absolute error values of BLAs are also given in relation to the MP2 reference data.

3.1. Molecular Structures. The ground-state equilibrium structure of five-double-bond conjugated models *9,13-dimethyl*, *9-methyl*, *13-methyl*, and *locked-11.5* is fully planar, whereas it is slightly twisted around C10−C11 and C11═C12 bonds in *locked-11.7*. For *9,10-dimethyl* and *9,10,13-trimethyl* compounds planar C_s and twisted structures were considered. Model *locked-11.8*, due to high flexibility of an eight-membered ring, displays three different conformers located energetically close to each other.

The CASSCF-based BLA (Table 1) values are strongly overestimated for conjugated species when compared to methods that include dynamic correlation energy and thus provide by far the largest BLA (0.097−0.122 Å for models under study) of all investigated methods. This is in agreement with previous findings for similar systems,[54] indicating that the CASSCF level of theory overestimates the difference in single

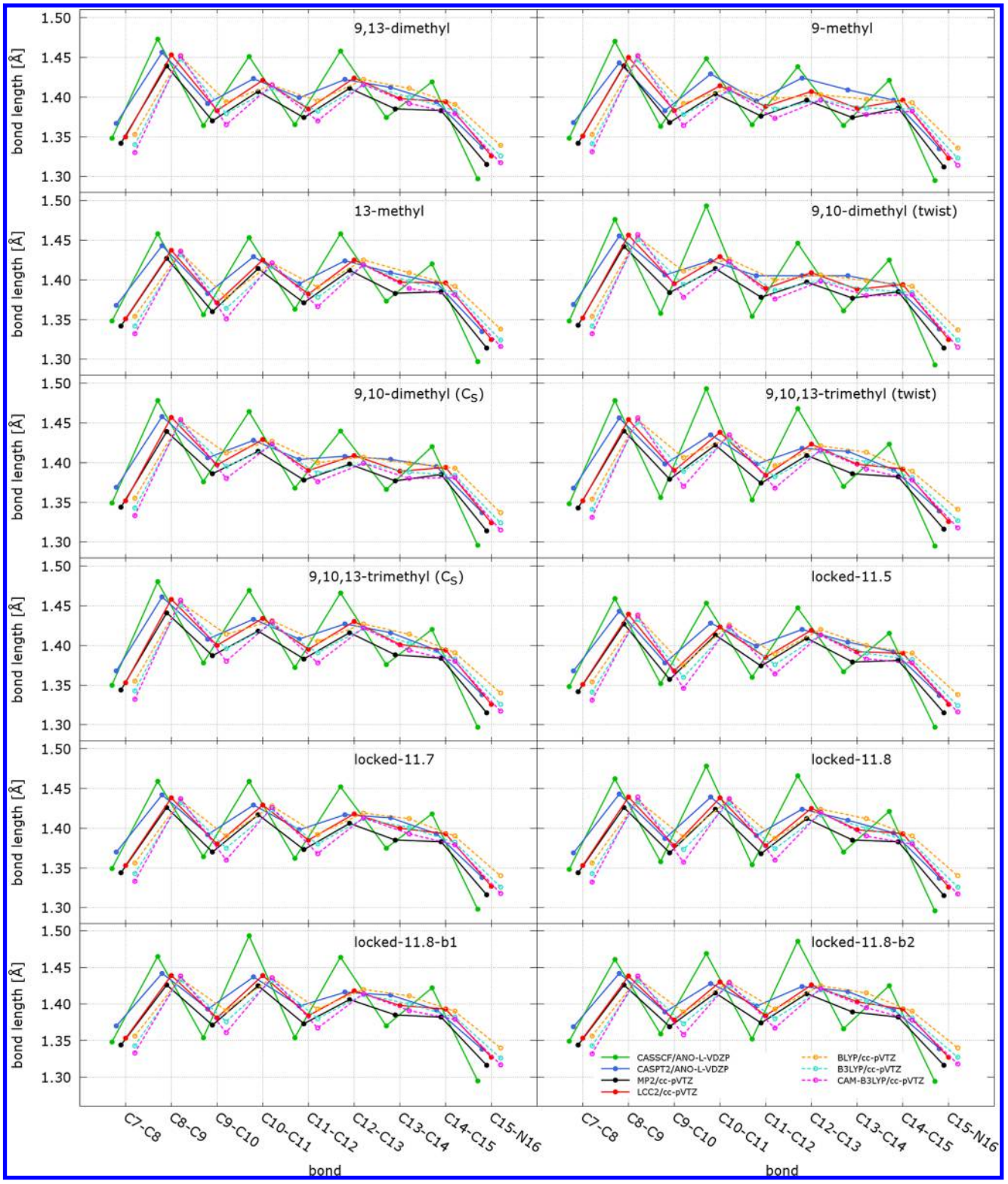

Figure 2. Comparison of the bond length alternation (BLA) pattern of the ground state of the retinyl chain of RPSB analogues calculated at various levels of theory.

and double bond lengths compared to the more accurate MRCI method. A more balanced description of single and double bonds may be obtained by other ab initio methods, namely, CASPT2, MP2, and LCC2. Indeed, the reduction in BLA gained due to inclusion of the dynamic correlation energy for most investigated systems exceeds 50%. CASPT2/ANO-L-VDZP bond lengths are found in satisfactory agreement with those of the MP2 and LCC2 as the mean absolute error (MAE) for CASPT2 and LCC2, with respect to MP2 values, is 0.011 and 0.002 Å, respectively.

The basis set effect on the ground-state bond distances and BLA values of various models obtained at CASSCF and

Table 2. Relative Energies (kcal/mol) with Respect to the *Twist* Structures Are Given as Well as Rotation around C10−C11 (C9−C10−C11−C12 Dihedral) and C11═C12 (C10−C11−C12−C13 Dihedral) Bonds of the *Twist* Models (deg)

	9,10-dimethyl			9,10,13-trimethyl		
	$E_{C_s}-E_{twist}$	C10−C11	C11═C12	$E_{C_s}-E_{twist}$	C10−C11	C11═C12
CASSCF/6-31G(d)	2.57	−122.1	4.9	11.29	−99.4	3.2
CASSCF/ANO-L-VDZP	2.13	−117.3	4.2	11.11	94.3	−2.4
CASPT2/6-31G(d)	0.94	−159.7	15.5	7.53	−97.1	3.5
CASPT2/ANO-L-VDZP	0.03	−167.9	9.9	9.31	−159.6	27.0
MP2/cc-pVTZ	0.48	−169.3	8.3	7.67	−159.8	25.4
LCC2/cc-pVTZ	−0.06	−165.9	11.6	6.50	−157.8	24.0
BLYP/cc-pVTZ	0.28	−171.7	5.3	5.12	−163.3	27.4
B3LYP/cc-pVTZ	0.37	−170.6	5.9	5.61	−161.9	25.9
CAM-B3LYP/cc-pVTZ	0.56	−168.0	7.6	6.45	−157.7	22.9

CASPT2 levels of theory is presented in Table S1 in the Supporting Information. Interestingly, for CASSCF, almost no change was observed between geometries optimized using 6-31G(d) and ANO-L-VDZP basis sets, as confirmed by the same values of CC and CN bond distances as well as MAE (see Table 1). On the contrary, CASPT2 structures are notably affected by basis set expansion, decreasing the BLA upon improving the basis set from 6-31G(d) to ANO-L-VDZP. Specifically, the double C═C and C═N bonds become elongated and the change is ca. 0.010 Å, whereas the single C−C bonds remain basically intact with the changes not exceeding 0.003 Å. Comparison of CASSCF/ANO-L-VDZP and CASPT2/ANO-L-VDZP geometries (see Figure 2) shows that double bonds become elongated and single bonds become shortened by 0.01−0.03 Å or even 0.05 Å in *locked-11.8-b1*, *locked-11.8-b2*, and twisted *9,10-dimethyl* and *9,10,13-trimethyl*. MP2/cc-pVTZ geometries feature a BLA 0.010−0.016 Å higher than that of CASPT2/ANO-L-VDZP, and all bonds in PSB5 models become shorter by 0.011−0.026 Å with the largest discrepancy, in most models, found at the ends of the PSB chain. However, a similar comparison of the structural parameters of *locked-11.5* obtained using the cc-pVDZ (or cc-pVTZ) basis set in both methods yields BLAs within 0.005 Å. (see Table S2 and Figure S1 in the Supporting Information). Moreover, a strong contraction of all bonds, up to 0.020 Å, was noticed when changing the basis set from double-ζ to triple-ζ quality. This is in line with the findings by Page and Olivucci,[28] who demonstrated a dramatic basis-set dependence of CASPT2 geometries in the ground and excited electronic states of small organic compounds. Therefore, it seems obvious that one would need to perform CASPT2/cc-pVTZ geometry optimization to bring CASPT2/ANO-L-VDZP molecular structures of retinals in even closer agreement with MP2/cc-pVTZ ones. LCC2 bond distances are in between MP2 and CASPT2 values; however, the BLA is in better agreement with MP2 (MAE is only 0.002 Å with respect to the MP2 reference value).

Among the DFT methods used for relaxation of retinal structures, B3LYP clearly outperforms CAM-B3LYP and BLYP and provides the structure similar in quality to the MP2 structure (MAE of only 0.003 Å). PBE0 results, presented in Tables S8−S15 in the Supporting Information, are essentially identical to B3LYP ones and, therefore, will not be discussed in the present paper. In fact, as pointed out by Wanko et al.,[55] hybrid functional B3LYP profits from the fortuitous error cancellation. On the contrary, general gradient approximation (GGA) methods, such as BLYP, featuring a dominating dynamic correlation term, tend to decrease BLA. Indeed, BLYP-based BLAs are ca. 0.011 Å lower than that of MP2, whereas CAM-B3LYP slightly overestimates them. Overall, B3LYP, CAM-B3LYP, BLYP, LCC2, and CASPT2/ANO-L-VDZP BLAs are within 0.016 Å of MP2 values for various retinal analogues, proving that each of the aforementioned methods provides a much better description of the ground-state structure of retinal analogues than does CASSCF for which the deviation from the MP2 BLA value is as large as 0.066 Å (0.082 Å relative to the CASPT2 value) for the *9,10-dimethyl* twisted structure.

3.2. Stability of Planar Structures. The effect of the level of theory applied in the geometry optimization procedure can also be noticed in the stability of the planar structure of the chromophore. Two of the systems investigated, namely, *9,10-dimethyl* and *9,10,13-trimethyl*, have methyl groups attached to the neighboring positions C9 and C10. These groups constitute enough of a sterical hindrance to destabilize the planarity of the system. The torsional deformation and relative energies of planar and twisted ground-state structures are compiled in Table 2. At the CASSCF/ANO-L-VDZP level, the global minimum geometry of *9,10-dimethyl* is mainly characterized by −117° torsional deformation of C9−C10−C11−C12, with the associated energy difference of 2.13 kcal mol^{-1} favoring the twisted structure. Inclusion of the dynamical correlation energy by means of CASPT2/ANO-L-VDZP diminishes the energy difference to just 0.03 kcal mol^{-1} and partially restores the planarity as the twist around the C10−C11 bond is −168°. One can notice the close resemblance of CASPT2 global and local minima structures to the ones obtained by MP2, LCC2, and DFT methods. Also, the CASPT2-, MP2-, and DFT-based relative energy of both minima ranges between 0.03 and 0.94 kcal/mol. Interestingly, while the LCC2 method predicts the twisting of the C9···C13 fragment in line with CASPT2 and MP2 methods, the energy difference is decreased to −0.06 kcal mol^{-1}, suggesting a planar structure as the very shallow global minimum.

Similar to *9,10-dimethyl*, the ground-state global minimum of *9,10,13-trimethyl* displays a twisted structure that must result from steric interactions between methyl substituents. However, the twisting of the C10−C11 and C11═C12 bonds is further increased by ca. 10° and 20° (at the CASPT2/ANO-L-VDZP level of theory), with respect to the corresponding values for *9,10-dimethyl*. The *9,10,13-trimethyl* chromophore structure maintains the same degree of twisting of the polyene chain throughout the CASPT2/ANO-L-VDZP, MP2, LCC2, and DFT levels of theory. In contrast, the CASSCF structure features a C10−C11 bond (twisting angle = −99°) that does not conjugate with the remaining part of the π system. The

twisted and unconjugated structure of CASSCF is preserved at the CASPT2/6-31G(d) level, affecting other structural and spectral properties. For instance, the *9,10,13-trimethyl* is the only model that displays much larger BLA at the CASPT2/6-31G(d) level (0.091 Å) compared to other structures. This is because the structure of *9,10,13-trimethyl* at CASPT2/6-31G(d) resembles the CASSCF structure better than the CASPT2/ANO-L-VDZP one. The difference found at CASSCF/ANO-L-VDZP (11.1 kcal mol^{-1}) is shifted down by 1.8 kcal mol^{-1} at CASPT2/ANO-L-VDZP, 3.4 kcal mol^{-1} at MP2, 4.6 kcal mol^{-1} at LCC2, and by 4.7−6.0 kcal mol^{-1} at DFT depending on the functional.

3.3. Conformers of *locked-11.8* Chromophore Models. Ring locks of various sizes lead to a different degree of torsional flexibility. Whereas, in planar five-membered and seven-membered ring structures, a single conformer appears, in *locked-11.8*, a ring strain induces an out-of-plane deformation of the PSB chain, resulting in three conformers: a half-chair (*locked-11.8*) and two boat conformations (*locked-11.8-b1*, *locked-11.8-b2*).

Analysis of the structural parameters of the three conformers of *locked-11.8* (see Table S3, Supporting Information) reveals that the choice of the level of theory used for geometry optimization can strongly affect the conformation of the ring, the twist of the central double bond, and, as a consequence, the spectral properties of the model. However, despite minor differences, CASSCF geometry of a half-chair conformation nicely correlates with the CASPT2 one, yielding the most significant deviations for C10−C11−C12−C13 (15°) and D−C10−C11−C12 torsions (12°). It is apparent from Figure 3 that this trend does not hold for boat conformations, which display a significantly bent conjugated backbone at the CASSCF/ANO-L-VDZP level, in line with the CASSCF/6-31G(d) calculations by De Vico et al.[24] that dramatically flattens upon upgrading the level of theory to CASPT2/ANO-L-VDZP. In the *locked-11.8-b1* conformer, the torsions that are mostly affected by the inclusion of the dynamic correlation at the CASPT2 level are C−D−C10−C11 and D−C10−C11−C12 (they become reduced by 44° and 42°, respectively), whereas, in the *locked-11.8-b2* conformer, C11−C12−C13−A and C12−C13−A−B torsions are both decreased by 37°. As shown in Table S3 (Supporting Information), the amount of torsional rotation in the chairlike conformer produced by a variety of methods, such as CASPT2, MP2, and LCC2, is practically identical. Such a close correlation between the CASPT2, MP2, and LCC2 results also holds true for both boat conformers. It can be seen that DFT functionals give a very good description of geometrical parameters of all three conformers as compared to highly correlated methods. On the other hand, CASSCF seems to produce the less accurate torsional deformation of *locked-11.8* conformers among all the methods investigated in this paper.

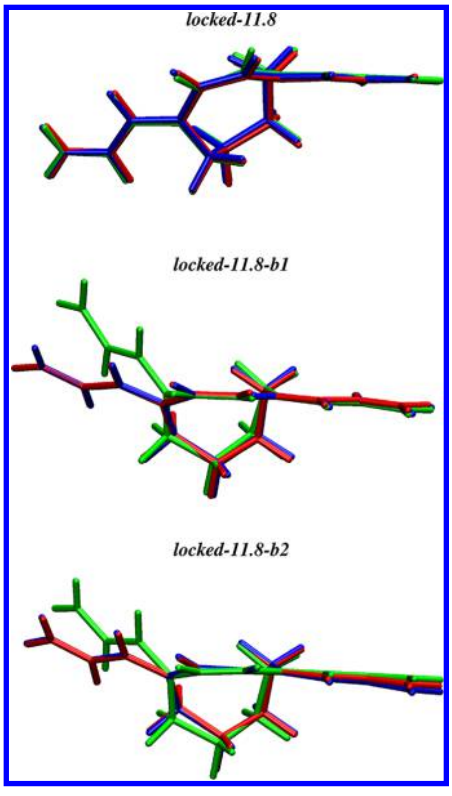

Figure 3. Superposition of *locked-11.8* conformer structures obtained at the CASPT2/ANO-L-VDZP (in blue), CASSCF/ANO-L-VDZP (in green), and MP2/cc-pVTZ (in red) levels of theory.

De Vico et al.[24] found all conformers located within a 1 kcal mol^{-1} energy range at the CASSCF/6-31G(d)/CASPT2/6-31G(d) level of theory with *locked-11.8-b2* being the most stable one, and the following energy order was predicted: *locked-11.8-b2* (−0.8 kcal mol^{-1}), *locked-11.8* (0.0 kcal mol^{-1}), and *locked-11.8-b1* (0.2 kcal mol^{-1}). According to our CASPT2/ANO-L-VDZP calculations (see Table 3), *locked-11.8-b1* appears to be the most stable one (−1.23 kcal mol^{-1}), followed by *locked-11.8-b2* (−0.50 kcal mol^{-1}), and finally *locked-11.8* (0.0 kcal mol^{-1}). The same energy order was found at the MP2 level of theory, reproducing the ca. 0.7 kcal mol^{-1} CASPT2-based energy gap between two boat conformers.

Table 3. Relative Energies (kcal/mol) of *locked-11.8* and *locked-11.8-b2* Conformers in Relation to *locked-11.8-b1*

	locked-11.8	*locked-11.8-b2*
CASSCF/6-31G(d)	2.70	0.25
CASSCF/ANO-L-VDZP	1.13	0.19
CASPT2/6-31G(d)	1.13	0.75
CASPT2/ANO-L-VDZP	1.23	0.73
MP2/cc-pVTZ	1.68	0.62
LCC2/cc-pVTZ	1.39	0.04
BLYP/cc-pVTZ	0.93	0.21
B3LYP/cc-pVTZ	1.23	0.27
CAM-B3LYP/cc-pVTZ	1.36	0.34

Interestingly, independently of the functional and hybrid or GGA scheme employed, DFT puts the conformers in the same order as CASPT2 and MP2 methods did. In the cases of DFT and LCC2, the separation between these conformations is underestimated, by up to 0.4−0.5 and 0.7 kcal mol^{-1}, respectively.

3.4. Vertical Excitation Energies. The basis set effect on CASPT2 excitation energies was tested by performing CASPT2 single-point calculations on the S_0 equilibrium structure of *locked-11.5* obtained at the CASPT2/ANO-L-VDZP level of theory. We employ the (aug)-cc-pVTZ and ANO-type basis sets. The deviations in the excitation energies from the standard CASPT2/ANO-L-VDZP results are given in Table 4. Although this is not an exhaustive search for an optimal basis set in CASPT2 energetics, some key features can be identified here.

Table 4. Deviations in the Excitation Energies from the SS-CASPT2/0-IPEA/ANO-L-VDZP Results Calculated at the FC Point for *locked-11.5*, Using the Basis Set Indicated in the Table.[c] Number of Primitive/Contracted Basis Functions and CPU Time Are Also Given

	ANO-L-VDZP	ANO-L-VTZP′[a]	ANO-L-VQZP′[b]	cc-pVTZ	aug-cc-pVTZ
no. functions	955/214	955/361	1501/674	721/498	1061/782
energy	0.00	0.01	0.00	0.05	0.01
CPU time	2	4	13	5	10

[a]Contraction scheme of ANO-L-VTZP′ basis set: [3s2p] for H and [4s3p2d] for C and N atoms. ANO-L-VTZP′ lacks 1d and 1f polarization functions on H and C, N, respectively, as compared to the original ANO-L-VTZP. [b]Contraction scheme of ANO-L-VQZP′ basis set: [3s2p1d] for H and [5s4p3d2f] for C, N atoms. ANO-L-VQZP′ notation is used as this basis set consists of the ANO-L-VTZP for H and ANO-L-VQZP for C and N atoms. [c]Geometries optimized at the CASPT2/ANO-L-VDZP level. Energies are given in eV, relative to the ANO-L-VDZP basis set.

Table 5. SS-CASPT2/ANO-L-VDZP Vertical $S_0 \rightarrow S_1$ Excitation Energies (eV) Based on a Two-Root SA-CASSCF Wave Function, Using the Geometry and Basis Set Indicated in the Table. CASPT2 Values Are Listed for Two Different IPEA Shifts: 0.0 and 0.25 au[b]

	CASSCF	CASPT2	MP2	BLYP	B3LYP	CAM-B3LYP
model	ANO[a]		cc-pVTZ			
			S-IPEA			
9,13-dimethyl	2.82	2.72	2.77	2.65	2.72	2.78
9-methyl	2.74	2.64	2.76	2.65	2.72	2.78
13-methyl	2.91	2.80	2.87	2.76	2.83	2.89
9,10-dimethyl (*twist*)	2.67	2.64	2.80	2.67	2.75	2.81
9,10-dimethyl (C_s)	2.79	2.69	2.76	2.64	2.72	2.78
9,10,13-trimethyl (*twist*)	2.79	2.52	2.62	2.53	2.60	2.66
9,10,13-trimethyl (C_s)	2.71	2.62	2.67	2.57	2.64	2.69
locked-11.5	2.80	2.69	2.77	2.70	2.76	2.80
locked-11.7	2.80	2.71	2.79	2.67	2.74	2.80
locked-11.8	2.71	2.58	2.66	2.58	2.65	2.71
locked-11.8-b1	2.76	2.65	2.71	2.62	2.69	2.74
locked-11.8-b2	2.66	2.58	2.65	2.59	2.65	2.70
mean absolute error	0.05	0.08		0.10	0.03	0.03
max absolute error	0.17	0.16		0.13	0.05	0.05
min absolute error	0.01	0.05		0.07	0.00	0.01
			0-IPEA			
9,13-dimethyl	2.47	2.38	2.43	2.32	2.38	2.44
9-methyl	2.41	2.32	2.43	2.33	2.40	2.45
13-methyl	2.57	2.47	2.54	2.43	2.50	2.56
9,10-dimethyl (*twist*)	2.36	2.30	2.46	2.33	2.40	2.47
9,10-dimethyl (C_s)	2.44	2.35	2.42	2.31	2.38	2.43
9,10,13-trimethyl (*twist*)	2.51	2.17	2.26	2.18	2.24	2.29
9,10,13-trimethyl (C_s)	2.35	2.27	2.32	2.22	2.29	2.34
locked-11.5	2.46	2.35	2.42	2.35	2.41	2.44
locked-11.7	2.45	2.38	2.44	2.33	2.39	2.45
locked-11.8	2.36	2.22	2.30	2.23	2.31	2.36
locked-11.8-b1	2.42	2.30	2.35	2.27	2.33	2.38
locked-11.8-b2	2.32	2.24	2.30	2.23	2.29	2.34
mean absolute error	0.06	0.08		0.10	0.03	0.02
max absolute error	0.25	0.16		0.13	0.13	0.05
min absolute error	0.01	0.05		0.07	0.07	0.01

[a]ANO stands for ANO-L-VDZP basis set. [b]Mean, maximum, and minimum absolute errors (in eV) of vertical excitation energies calculated for different geometries when corresponding MP2 is taken as a reference.

The shift in excitation energy due to the ANO-L basis set extension up to ANO-L-VTZP′ and ANO-L-VQZP′ remains within 0.01 eV. The cc-pVTZ excitation energies agree within 0.05 eV with the excitation energies calculated using ANO-L-VDZP. However, the inclusion of diffusion functions to cc-pVTZ decreases the energy by 0.04 eV, giving the same energy as the ANO-L-VTZP′ basis set, only 0.01 eV away from ANO-L-VDZP. In light of the above results, the ANO-L-VDZP basis set seems to be an appropriate and cost-efficient choice to carry out CASPT2 calculations of excitation energies in cationic PSB models.

To account for the impact of the ground-state geometry obtained with various methods on the $S_0 \rightarrow S_1$ excitation energy in RPSB models, we performed CASPT2/ANO-L-VDZP single-point energy calculations, using the two-root state-average CASSCF (SA-CASSCF) wave function and full π active space, based on CASSCF, CASPT2, MP2, and DFT (BLYP, B3LYP, CAM-B3LYP) S_0 equilibrium geometries. The

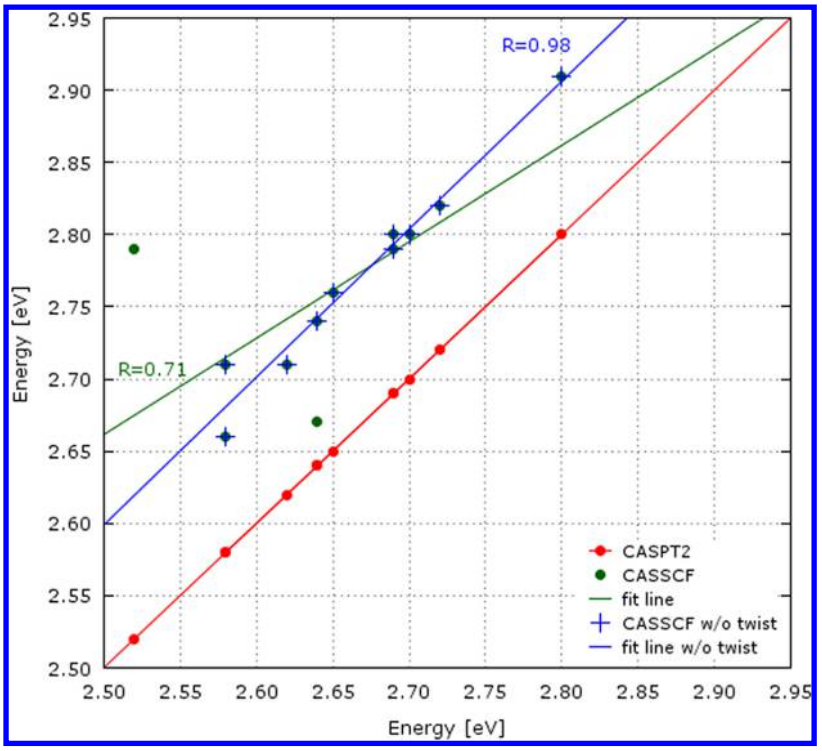

Figure 4. Correlation plot for the vertical excitation energies (eV) from the CASSCF/SS-CASPT2/ANO-L-VDZP method with respect to the CASPT2/ANO-L-VDZP reference values. S-IPEA was used in all calculations. The blue line was produced taking into consideration planar structures only. The green line was produced taking into account all planar and two twisted structures.

Table 6. The Lowest $S_0 \rightarrow S_1$ Vertical Excitation Energies (eV) for RPSB Analogues Calculated at Various Levels of Theory[d]

	CASPT2			CC2	LCC2[a]	TD-BLYP	TD-B3LYP	TD-CAM-B3LYP
model	6-31G(d)	ANO[b]	ref[c]			cc-pVTZ		
9,13-dimethyl	2.79	2.72	2.77	2.77	2.80 (2.41)	2.82	2.94	3.03
9-methyl	2.72	2.64	2.76	2.78	2.76 (2.43)	2.83	2.95	3.03
13-methyl	2.87	2.80	2.87	2.91	2.89 (2.51)	2.89	3.04	3.17
9,10-dimethyl (*twist*)	2.70	2.64	2.80	2.79	2.74 (2.33)	2.83	2.95	3.03
9,10-dimethyl (C_s)	2.76	2.69	2.76	2.75	2.79 (2.37)	2.81	2.93	3.00
9,10,13-trimethyl (*twist*)	2.74	2.52	2.62	2.59	2.48 (2.15)	2.67	2.78	2.86
9,10,13-trimethyl (C_s)	2.68	2.62	2.67	2.62	2.66 (2.27)	2.63	2.78	2.89
locked-11.5	2.79	2.69	2.77	2.80	2.78 (2.42)	2.79	2.94	3.08
locked-11.7	2.78	2.70	2.79	2.79	2.68 (2.34)	2.78	2.93	3.05
locked-11.8	2.67	2.58	2.66	2.64	2.57 (2.20)	2.71	2.84	2.95
locked-11.8-b1	2.71	2.65	2.71	2.71	2.57 (2.26)	2.70	2.86	2.98
locked-11.8-b2	2.65	2.58	2.65	2.65	2.52 (2.20)	2.68	2.84	2.95
mean absolute error	0.03	0.08		0.02	0.06 (0.41)	0.04	0.16	0.27
max absolute error	0.12	0.16		0.05	0.14 (0.47)	0.07	0.19	0.31
min absolute error	0.00	0.05		0.00	0.00 (0.33)	0.01	0.11	0.22

[a]LCC2-based vertical excitation energies were calculated using augmented domains. In parentheses, there are values of excitation energies using standard domains. [b]ANO stands for ANO-L-VDZP basis set. [c]SS-CASPT2/ANO-L-VDZP (S-IPEA) excitation energies at the MP2/cc-pVTZ equilibrium geometries. For *locked-11.5*, SS-CASPT2/S-IPEA/ANO-L-VDZP excitation energy at the CASPT2/cc-pVTZ equilibrium geometry is 2.74 eV. [d]CASPT2 values are obtained as SS-CASPT2 using IPEA-shift = 0.25 au. Mean, maximum, and minimum absolute errors (in eV) of vertical excitation energies calculated with respect to CASPT2/ANO results.

single-state (SS) and multistate (MS) CASPT2 excitation energies employing both the standard IPEA (S-IPEA) and the previously used null IPEA (0-IPEA) zero-order Hamiltonian are reported in Table 5 (SS-CASPT2 results) and Table S4 (Supporting Information) (MS-CASPT2 results). As can be readily seen from these results, SS- and MS-CASPT2 energies are within 0.04 eV for CASSCF, CASPT2, and MP2 geometries, and this gap is not significantly changed when other geometries are employed. On the other hand, the usage of the IPEA-shift is responsible for a systematic ca. 0.3 eV upshift of the $S_0 \rightarrow S_1$ energy regardless of the level of theory utilized to obtain the geometry. This trend is observed for all investigated RPSB models and further validates similar findings by Valsson, Angeli, and Filippi for full RPSB.[27] To understand how the number of roots does affect the CASPT2 excitation energies, we also ran calculations for three roots and deposited the results in the Supporting Information (Tables S5 and S6). It turns out that the excitation energies based on the two-root

SA-CASSCF wave function are higher by 0.01−0.04 eV regardless of the ground-state geometry chosen.

It has become a common practice in photochemical studies to estimate the excitation energy from CASSCF/CASPT2 calculations.[23,24,56,57] That means that the geometry is optimized at the relatively cheaper CASSCF level of theory, followed by a single-point CASPT2 calculation of the excited-state energies. In the following paragraph, we show that this procedure yields good results; however, there is still plenty of room for improvements. The CASSCF excitation energies are overestimated by 0.52−0.79 eV, compared to CASSCF/CASPT2. The CASSCF/CASPT2 level of theory yields quite accurate excitation energies, changing by less than 0.11 eV, compared with respective CASPT2 calculations. Indeed, a correlation between CASPT2/ANO-L-VDZP excitation energies based on CASSCF and CASPT2 geometries, displayed in Figure 4, reveals that the excitation energies from CASSCF geometry tend to be, on average, 0.1 eV higher than those from CASPT2 geometry, highlighting a systematic deviation over the whole range of data. It seems that the error introduced by the lack of the dynamic correlation energy during the CASSCF optimization procedure is systematic for the systems studied here, at least for planar structures, and an a posteriori correction of approximately −0.1 eV to the vertical excitation energies calculated at the CASSCF/CASPT2 level of theory will lead to the results in perfect agreement with the reference CASPT2 values. However, this deviation increases to as much as 0.27 eV for the twisted *9,10,13-trimethyl* model, raising serious concerns about the use of the CASSCF methodology to search for minima corresponding to different torsional conformations. An augmentation of the basis set from 6-31G(d) to ANO-L-VDZP in CASSCF/CASPT2 and CASPT2 calculations yields a ca. 0.05−0.10 eV downshift of the excitation energies.

CASPT2 excitation energies calculated at the MP2 equilibrium geometries are regarded as the reference data in this work since CASPT2 optimization in the cc-pVTZ basis set was not feasible except for the smallest model: *locked-11.5*. The close agreement between CASPT2/cc-pVTZ and MP2/cc-pVTZ geometries results in just a 0.03 eV energy difference between their corresponding CASPT2 excitation energies (see Table 6). As expected, somewhat larger deviations (0.05−0.12 eV for all models, except for the twisted *9,10-dimethyl*) are observed when comparing excitation energies calculated at CASPT2/ANO-L-VDZP and MP2/cc-pVTZ geometries.

We find that B3LYP is a reliable method to calculate ground-state equilibrium geometries for retinal models, as reflected by its small maximum error (0.05 eV) in the excitation energies with respect to the MP2-based reference values. CAM-B3LYP, in the light of the overestimated BLA values, leads to blue-shifted excitation energies; however, mean and maximum absolute errors are the same as those derived from B3LYP results. Finally, BLYP displays less accurate equilibrium structures among DFT functionals, leading to excitation energies, which, for some systems, for example, *9,10-dimethyl* (twist), *9,13-dimethyl*, and *locked-11.7*, are at least 0.12 eV higher than their corresponding values computed at the MP2 geometry. It is evident at first sight that CASPT2, CASSCF, MP2, and DFT structures define a rather narrow range of excitations for RPSB models: the deviation among CASPT2 energies from geometries of different origins does not exceed 0.20 eV for planar chromophores but becomes 0.29 eV for the twisted *9,10,13-trimethyl* model. By comparing CASPT2 excitation energies at CASSCF-, CASPT2-, MP2-, and DFT-optimized geometries, one can notice a blue shift with increasing BLA: CASPT2, BLYP < B3LYP < MP2 < CAM-B3LYP < CASSCF. This noticeable impact of BLA on the absorption energy has been observed in *all-trans* retinal.[55]

A comparison of vertical excitation energies calculated at the same level of theory as the ground-state geometries is compiled in Table 6. The CASPT2 excitations were computed using the IPEA zero-order Hamiltonian (S-IPEA) as it has been shown to provide the best correlation with other high-level ab initio methods, such as CCSD, CC3, NEVPT2, or quantum Monte Carlo (QMC).[26] It is known that a good performance of the widely used CASPT2/0-IPEA protocol in predicting excitation energies for PSBs when using a limited basis set (6-31G(d)) and CASSCF-optimized geometries can be attributed to cancellation of errors.[26,29] We can also support Valsson and Filippi's[26] finding that S-IPEA excitations are less sensitive to the choice of single- or multistate scheme. Analysis of the data presented in Table 6 reveals a very good agreement of CC2 results with the CASPT2/ANO-L-VDZP excitation energies at MP2/cc-pVTZ-optimized geometries, which we consider here as the reference data, with the mean absolute error of 0.02 eV for all retinal models. The present result is in line with findings of Aquino et al.,[54] who demonstrated that the CC2 method performs quite well for PSB models when compared to MRCI. On the contrary, rather disappointing results are obtained employing the LCC2 scheme, yielding an MAE of more than 0.4 eV. However, LCC2 results practically converge to the CC2 excitation energies upon merging overlapping orbital domains (compare 0.02 eV MAE for CC2 and 0.06 eV MAE for LCC2). This difference may become larger for the full RPSB chromophore probably due to a different response of both approaches to the addition of the β-ionone ring, as indicated by Valsson et al.[27] The exact same behavior is observed for CC2 and CASPT2 excitation energies for the isolated chromophore optimized in the presence of MM charges by QM/MM MD simulations.[58]

When comparing TD-DFT excitation energies in cationic models of RPSB to the reference data provided by CASPT2 calculations utilizing MP2 geometries, a rather poor performance by the TD-DFT method should be noted with the maximum error ranging from 0.07 eV (for BLYP) to 0.31 eV (for CAM-B3LYP) (Table 6). The TD-DFT method employed in this study has well-known difficulties in describing the charge-transfer $S_0 \rightarrow S_1$ electron transition as well as energies of distorted structures,[55,59] for example, the largest deviation observed for *9,10-dimethyl* and *9,10,13-trimethyl* twisted structures in this study. Out of the four functionals utilized in this study, BLYP is by far the most successful one in reproducing CASPT2 excitation energies: the differences are between 0.01 eV for *locked-11.8-b1* and 0.07 eV for *9-methyl*, resulting in an MAE as low as 0.04 eV compared to 0.16 eV for B3LYP and 0.27 eV for CAM-B3LYP. The reason behind this surprisingly good performance of BLYP is an error cancellation resulting from underestimated BLA and TD-DFT tendency to overestimate charge transfer excitation energies in PSB5 models.

In the CASSCF and CASPT2 calculations, the lowest $\pi-\pi^*$ electron transition is dominated by single excitation from HOMO to LUMO (HOMO denotes highest occupied molecular orbital, and LUMO denotes lowest unoccupied molecular orbital). This conclusion is supported by both CC2 and DFT results.

Table 7. Oscillator Strength for the Lowest $S_0 \rightarrow S_1$ Vertical Excitation Calculated at Various Levels of Theory

	CASSCF[a]		CASPT2[b]			CC2[c]	LCC2[d]	BLYP[e]	B3LYP[e]	CAM-B3LYP[e]
model	6-31G(d)	ANO[f]	6-31G(d)	ANO[f]	ref[g]			cc-pVTZ		
9,13-dimethyl	1.13	1.15	1.49	1.54	1.49	1.47	1.51 (1.00)	1.17	1.29	1.35
9-methyl	1.01	1.00	1.35	1.38	1.33	1.34	1.37 (0.98)	1.09	1.20	1.25
13-methyl	1.12	1.14	1.48	1.53	1.47	1.53	1.56 (1.04)	1.13	1.32	1.41
9,10-dimethyl (*twist*)	0.29[h]	0.20[h]	1.35	1.56	1.53	1.46	1.38 (0.96)	1.16	1.28	1.32
9,10-dimethyl (C_s)	1.19	1.21	1.57	1.62	1.56	1.49	1.53 (1.06)	1.16	1.28	1.34
9,10,13-trimethyl (*twist*)	0.00[h]	0.01[h]	1.11[h]	1.40	1.30	1.18	1.08 (0.74)	1.01	1.07	1.06
9,10,13-trimethyl (C_s)	1.08	1.10	1.48	1.56	1.47	1.38	1.43 (0.94)	0.95	1.14	1.24
locked-11.5	0.71	0.70	0.92	0.91	0.89	0.84	0.85 (0.61)	0.60	0.71	0.78
locked-11.7	1.11	1.13	1.50	1.55	1.47	1.36	1.32 (0.94)	0.98	1.16	1.26
locked-11.8	0.69	0.70	1.16	1.25	1.24	1.08	1.05 (0.70)	0.90	1.00	1.01
locked-11.8-b1	0.36[h]	0.35[h]	1.34	1.46	1.39	1.23	1.14 (0.82)	0.87	1.05	1.12
locked-11.8-b2	0.38	0.38	1.23	1.42	1.36	1.21	1.14 (0.81)	0.87	1.06	1.12

[a]Two-root SA-CASSCF wave function and SS-CASPT2/S-IPEA excitation energy at the CASSCF-optimized geometry were used to obtain oscillator strengths. [b]Two-root SA-CASSCF wave function and SS-CASPT2/S-IPEA excitation energy at the CASPT2-optimized geometry were used to obtain oscillator strengths. [c]CC2-based oscillator strengths obtained at MP2-optimized geometry. [d]LCC2-based oscillator strengths were calculated using augmented domains. In parentheses, there are values of oscillator strengths using standard domains. [e]TD-DFT calculations. [f]ANO stands for ANO-L-VDZP basis set. [g]Two-root SA-CASSCF wave function and SS-CASPT2/ANO-L-VDZP/S-IPEA excitation energy at the MP2/cc-pVTZ-optimized geometry were used to obtain oscillator strengths. For *locked-11.5*, we additionally calculated oscillator strength (0.91) by using the two-root SA-CASSCF/ANO-L-VDZP wave function and SS-CASPT2/S-IPEA/ANO-L-VDZP excitation energy at the CASPT2/cc-pVTZ-optimized geometry. [h]The oscillator strength for the $S_0 \rightarrow S_2$, calculated using the three-root SA-CASSCF wave function and SS-CASPT2/S-IPEA excitation energy, has a larger mangnitude than the one for the $S_0 \rightarrow S_1$ transition and is 0.76 (0.82), 1.01 (1.03), and 0.68 (0.66) for CASSCF/6-31G(d) (CASSCF/ANO-L-VDZP) geometries in the cases of *9,10-dimethyl* (twist), *9,10,13-trimethyl* (twist), and *locked-11.8-b1*, respectively.

Table 8. Change in Dipole Moment (D) for the Lowest $S_0 \rightarrow S_1$ Vertical Excitation Calculated at Various Levels of Theory

	CASSCF[a]		CASPT2[b]			CC2[c]	LCC2[d]	BLYP[e]	B3LYP[e]	CAM-B3LYP[e]
model	6-31G(d)	ANO[f]	6-31G(d)	ANO[f]	ref[g]			cc-pVTZ		
9,13-dimethyl	13.11	12.57	10.22	8.96	9.53	5.40	2.20 (2.57)	0.55	1.21	2.47
9-methyl	12.08	11.68	9.08	8.11	8.61	4.91	1.96 (2.20)	0.47	1.05	2.17
13-methyl	11.02	10.60	8.88	8.21	8.44	6.28	2.47 (2.81)	1.06	1.79	3.10
9,10-dimethyl (*twist*)	11.36	10.40	9.21	7.22	8.74	4.67	1.98 (2.05)	0.44	0.97	2.07
9,10-dimethyl (C_s)	13.32	12.80	9.36	8.02	8.83	4.55	1.98 (2.04)	0.35	0.92	2.01
9,10,13-trimethyl (*twist*)	9.09	8.51	7.99	8.16	8.99	5.13	2.45 (2.81)	0.61	1.31	3.03
9,10,13-trimethyl (C_s)	14.03	13.53	10.74	9.70	10.27	6.29	2.65 (3.03)	0.72	1.62	3.25
locked-11.5	8.37	8.07	5.77	5.05	5.41	3.00	1.22 (1.32)	0.85	1.28	2.05
locked-11.7	11.55	11.15	9.06	8.18	8.89	5.79	2.39 (2.58)	1.03	1.74	3.00
locked-11.8	11.24	10.84	9.55	8.36	8.88	5.50	2.44 (2.71)	0.89	1.61	3.26
locked-11.8-b1	9.35	8.88	8.53	7.70	8.09	5.57	2.39 (2.56)	1.07	1.77	3.15
locked-11.8-b2	10.16	9.79	8.88	7.71	8.11	5.18	2.33 (2.43)	1.05	1.70	3.05

[a]Two-root SA-CASSCF wave function at the CASSCF-optimized geometry was used to obtain dipole moments. [b]Two-root SA-CASSCF wave function at the CASPT2-optimized geometry was used to obtain dipole moments. [c]CC2-based dipole moments obtained at MP2-optimized geometry. [d]LCC2-based dipole moments were calculated using augmented domains. In parentheses, there are values of dipole moments using standard domains. [e]TD-DFT calculations. [f]ANO stands for ANO-L-VDZP basis set. [g]Two-root SA-CASSCF wave function at the MP2/cc-pVTZ-optimized geometry was used to obtain dipole moments For *locked-11.5*, we additionally obtained the change in dipole moment (5.17 D) by using the two-root SA-CASSCF/ANO-L-VDZP wave function at the CASPT2/cc-pVTZ-optimized geometry.

3.5. Oscillator Strengths. For all RPSB models, except *9,10,13-trimethyl* (twist), the transition to the S_1 state is strongly dipole-allowed. According to the results collected in Table 7, oscillator strengths are very sensitive to the choice of the methodology but do not depend strongly on the basis set. There is a noticeable trend that CASPT2/ANO-L-VDZP, CASPT2 at MP2/cc-pVTZ geometry, CC2, and LCC2 (with merged domains scheme), which agree well with each other, are the largest, followed by TD-DFT/CAM-B3LYP, TD-DFT/B3LYP, and TD-DFT/BLYP. In going from CASSCF to CASPT2 geometry, the oscillator strengths change dramatically by rising up to 40%. This change can be negatively correlated to BLA: the decrease of BLA when going from CASSCF to CASPT2 leads to higher oscillator strengths. On the contrary, a comparison of DFT results displays a completely different picture with CAM-B3LYP producing the largest BLA and the largest oscillator strength, followed by B3LYP and BLYP. Oscillator strengths are also sensitive to the degree of twisting of the polyene chain as planar *9,10-dimethyl* and *9,10,13-trimethyl* have larger oscillator strengths than their twisted counterparts regardless of the method employed, with the exception of BLYP. The largest variation in the computed oscillator strengths between planar and twisted structures is observed at the CASSCF level. In fact, in the cases of the twisted *9,10,13-trimethyl* and *9,10-dimethyl* as well as *locked-11.8-b1* models, the CASSCF results imply that the $S_0 \rightarrow S_2$ transition and not the $S_0 \rightarrow S_1$ is identified as the brightest one.

Among the locked models, the *locked-11.7* has the largest oscillator strength, whereas it is reduced for *locked-11.8* and even more for *locked-11.5*, regardless of the method used. Despite the fact that the excitation energies of the *locked-11.8* conformers are similar, they have different oscillator strengths: larger for the pseudochair conformer and lower for the pseudoboat conformers at CASSCF and TD-BLYP levels of theory. Other methods provide a different picture with boat conformers having more bright $S_0 \rightarrow S_1$ transition than the chair conformer. These values correlate well with the stability of the conformers.

Comparison of CC and B3LYP oscillator strengths for valence excitations in DNA bases reveals that B3LYP values are smaller than their CC counterparts.[60] In addition, the recent papers by Thiel's group[61,62] state that B3LYP outperforms the BLYP functional in a study based on a large number of excited states for 28 benchmark molecules. In the very extensive benchmark of oscillator strengths computed for alkenes, carbonyls, and azobenzenes by Caricato et al.,[63] the short−long-range separated functional CAM-B3LYP performs better than hybrid B3LYP and gradient-corrected BLYP functionals in reproducing CASPT2 and CC2 results. Results collected in Table 7 confirm all the above findings.

3.6. Dipole Moments. Dipole moments in the S_0 and S_1 states calculated at CASSCF, CASPT2, LCC2, CC2, and TD-DFT levels of theory are compiled in Table S7 in the Supporting Information, whereas the resulting changes in the dipole moments induced upon $S_0 \rightarrow S_1$ electron excitation are shown in Table 8. The most general conclusion is that the ground state has a significant dipole moment (up to 11 D at CASPT2 level), whereas the excitation to S_1 reduces the dipole moment to ca. 1−2 D. This is related to the charge flow accompanying the excitation, which was found by others.[23] The decrease of the dipole moment after excitation is explained very well by the Mulliken and NBO charge distribution (see Figure S2 in the Supporting Information). In general, in the ground state, there is a significant positive charge at the N16 end of the molecule; after the excitation to the S_1 state, the electrons are distributed more evenly along the molecule and the positive charge at the N16 end is reduced. The dynamic correlation added at the CASPT2 level does not change the charges much.

The level of theory applied has a large impact on the value of the change of the dipole moment upon $S_0 \rightarrow S_1$ excitation. The trend is that CASSCF values are always the highest; at the CASPT2 level, the change in the dipole moment is lower; and, at the coupled cluster level, it is reduced even more. Also, increasing the basis set size leads to reduction of the magnitude of the dipole moment. For instance, the change in the dipole moment for *9,13-dimethyl* is 13.1 D at CASSCF/6-31G(d), 12.6 D at CASSCF/ANO-L-VDZP, 10.2 D at CASPT2/6-31G(d), 9.0 D at CASPT2/ANO-L-VDZP, 5.4 D at the CC2/cc-pVTZ, and 2.6 D at LCC2/cc-pVTZ levels of theory. This trend is quite similar for all the models studied here. Interestingly, within the two-root SA-CASSCF formalism, the usage of the MP2-optimized geometry brings calculated values of the change in dipole moment for various models closer to those derived from CASPT2/6-31G(d) rather than CASPT2/ANO-L-VDZP geometry, reflecting a fortuitous agreement of MP2 and CASPT2/6-31G(d) BLAs.

LCC2 results have the lowest magnitude of the change in the dipole moment (ca. 50% lower than CC2 results) among ab initio methods considered in this work, hence reflecting a possible deficiency of the LCC2 method in describing the charge-transfer transitions regardless of the fact of whether or not augmented domains are used in the calculations. It comes as no surprise that TD-DFT cannot capture the charge-transfer character of the $S_0 \rightarrow S_1$ transition and has a tendency to overestimate the excited-state dipole moment (see Table S7, Supporting Information). Hybrid functionals, especially CAM-B3LYP, perform much better than BLYP does, but still, the change in the dipole moment predicted by TD-DFT/CAM-B3LYP is 3−6 D lower than CASPT2/ANO-L-VDZP values for various RPSB models.

Dipole moments, similar to oscillator strengths, are highly sensitive to the choice of the ground-state geometry. In fact, there is a negative correlation between BLA and the change in dipole moments for CASSCF and CASPT2, whereas it turns to be positive for DFT functionals. Some correlation with the planarity of the molecule might be observed: for the *9,10-dimethyl* and *9,10,13-trimethyl* models, as well as for the *boat* conformers of *locked-11.8*, the CASSCF level yields larger values of the change in the excited-state dipole moment for planar structures. At CASPT2 and CC2 levels, which predict more planar global minima than CASSCF does, the magnitude of the change in the dipole moment is reduced and becomes similar for planar and twisted structures.

4. CONCLUSIONS

The present work reports the first CASPT2/ANO-L-VDZP ground-state geometry optimization, followed by the CASPT2/ANO-L-VDZP vertical excitation energy calculation for methylated, demethylated, and locked models of RPSB chromophores without the β-ionone ring. We have also assessed the quality of CC2, LCC2, and TD-DFT vertical excitation energies with respect to the state-of-the-art CASPT2 data.

It has been shown that the CASSCF geometry differs significantly from geometries optimized with the dynamic correlation included. These differences comprise mostly the amount of bond length alternation and, in some cases, dihedral angles (e.g., in *locked-11.8*). Also, if the dynamic correlation is not included (e.g., CASSCF method), the highly twisted conformers of *9,10-dimethyl* and *9,10,13-trimethyl* species are found to be the global minima, whereas they turn to be nearly planar at the CASPT2, MP2, LCC2, and DFT levels of theory. An analysis of the CASPT2 results, both in terms of geometries and vertical excitation energies, reveals that they depend highly on the quality of the basis set utilized in the calculations. Consequently, the usage of the small 6-31G(d) basis may provide a completely wrong structure, like it happened here for the twisted *9,10,13-trimethyl* model. CASPT2 ground-state geometry reasonably correlates with other highly correlated ab initio methods CC2 and LCC2, as well as DFT.

The effect of the ground-state geometry on vertical excitation energies has been rationalized and has been shown to be of limited importance as CASPT2 calculated excitation energies based on geometries produced by such different methods as CASSCF, CASPT2, MP2, LCC2, and DFT are within 0.2 eV. As expected, the CASSCF level of theory largely overestimates the energy of the vertical excitations.[54] The CASSCF/CASPT2 level offers quite a good approximation for planar RPSB models but ends up with the large errors for strongly twisted structures, for example, *9,10,13-trimethyl*. In terms of the excitation energy, the following trend can be observed: the values of the excitation energy are decreased (improved), when the basis set size is increased and the dynamical correlation is included.

The approximate CC2 level of theory has shown a remarkable performance, manifested by a good agreement with the most accurate CASPT2/ANO-L-VDZP level of theory. LCC2 may provide the same level of accuracy, but vertical excitation energies and oscillator strengths produced by this method seem to be highly sensitive to the choice of domains. The TD-DFT framework using B3LYP and CAM-B3LYP functionals yields excitation energies of much lower accuracy, typically deviating by 0.3 eV from CASPT2 results. Surprisingly, TD-DFT/BLYP performs better, with a mean absolute error of only 0.04 eV, most likely due to fortuitous error cancellation.

To conclude, we believe that this CASPT2 benchmark set provides a solid reference and can be utilized for validation and development studies on RPSB analogues.

■ ASSOCIATED CONTENT

Supporting Information

Bond lengths of all models obtained at CASSCF and CASPT2 using 6-31G(d) and ANO-L-VDZP basis sets; bond lengths of locked-11.5 model calculated at MP2 and CASPT2 levels using various basis sets; calculated dipole moments in S_0 and S_1 states of all models; ground-state structural parameters, relative energies, and vertical excitation energies obtained using DFT (TD-DFT) with the PBE0 functional; Cartesian coordinates of optimized retinal models' geometries. This material is available free of charge via the Internet at http://pubs.acs.org.

■ AUTHOR INFORMATION

Corresponding Author

*E-mail: tadeusz.andruniow@pwr.wroc.pl.

Author Contributions

†E.W. and B.S. contributed equally to this work.

Notes

The authors declare no competing financial interest.

■ ACKNOWLEDGMENTS

This work was supported by Wroclaw Research Centre EIT+ within the project "Biotechnologies and advanced medical technologies" - BioMed (POIG.01.01.02-02-003/08) co-financed by the European Regional Development Fund (Operational Programme Innovative Economy, 1.1.2). We would like to thank Dr. Tatiana Korona for fruitful discussions on LCC2 calculations. Calculations were performed at the Wroclaw Supercomputer and Networking Center (WCSS) and the Academic Computer Center Cyfronet AGH in Krakow.

■ REFERENCES

(1) Polli, D.; Altoe, P.; Weingart, O.; Spillane, K. M.; Manzoni, C.; Brida, D.; Tomasello, G.; Orlandi, G.; Kukura, P.; Mathies, R. A.; Garavelli, M.; Cerullo, G. *Nature* **2010**, *467*, 440−443.

(2) Kim, J. E.; Tauber, M. J.; Mathies, R. A. *Biochemistry* **2001**, *40*, 13774−13778.

(3) Mathies, R.; Lugtenburg, J. In *Handbook of Biological Physics*; Stavenga, D., DeGrip, W., Pugh, E., Eds.; Elsevier Science: Amsterdam, 2000; Vol. 3, pp 55−90.

(4) Schick, G. A.; Cooper, T.; Holloway, R.; Murray, L.; Birge, R. *Biochemistry* **1987**, *26*, 2556−2562.

(5) Blatz, P. E.; Lin, M.; Balasubramaniyan, P.; Balasubramaniyan, V.; Dewhurst, P. B. *J. Am. Chem. Soc.* **1969**, *91*, 5930−5931.

(6) Nelson, R.; deRiel, J. K.; Kropf, A. *Proc. Natl. Acad. Sci. U.S.A.* **1970**, *66*, 531−538.

(7) Chan, W. K.; Nakanishi, K.; Ebrey, T. G.; Honig, B. *J. Am. Chem. Soc.* **1974**, *96*, 3642−3644.

(8) Mao, B.; Tsuda, M.; Ebrey, T.; Akita, H.; Balogh-Nair, V.; Nakatsuji, K. *Biophys. J.* **1981**, *35*, 543−546.

(9) Buchert, J.; Stefancic, V.; Doukas, A.; Alfano, R.; Callender, R.; Pande, J.; Akita, H.; Balogh-Nair, V.; Nakatsuji, K. *Biophys. J.* **1983**, *43*, 279−283.

(10) Weingart, O.; Schapiro, I.; Buss, V. *J. Phys. Chem. B* **2007**, *111*, 3782−3788.

(11) Sugihara, M.; Buss, V. *Biochemistry* **2008**, *47*, 13733−13735.

(12) Laricheva, E. N.; Gozem, S.; Rinaldi, S.; Melaccio, F.; Valentini, A.; Olivucci, M. *J. Chem. Theory Comput.* **2012**, *8*, 2559−2563.

(13) Kochendoerfer, G.; Verdegem, P.; van der Hoef, I.; Lugtenburg, J.; Mathies, R. *Biochemistry* **1996**, *35*, 16230−16240.

(14) Gärtner, W.; Ternieden, S. *J. Photochem. Photobiol., B* **1996**, *33*, 83−86.

(15) Wang, Q.; Kochendoerfer, G.; Schoenlein, R.; Verdegem, P.; Lugtenburg, J.; Mathies, R.; Shank, C. *J. Phys. Chem.* **1996**, *100*, 17388−17394.

(16) Koch, D.; Gärtner, W. *Photochem. Photobiol.* **1997**, *65*, 181−186.

(17) DeLange, F.; Bovee-Geurts, P.; VanOostrum, J.; Portier, M. D.; Verdegem, P.; Lugtenburg, J.; DeGrip, W. *Biochemistry* **1998**, *37*, 1411−1420.

(18) Jäger, F.; Lou, J.; Nakatsuji, K.; Atkinson, G. *J. Am. Chem. Soc.* **1998**, *120*, 3739−3747.

(19) Verdegem, P.; Bovee-Geurts, P.; de Grip, W.; Lugtenburg, J.; de Groot, H. *Biochemistry* **1999**, *38*, 11316−11324.

(20) Mizukami, T.; Kandori, H.; Shichida, Y.; Derguini, A.-H. C. F.; Caldwell, C.; Bigge, C.; Nakatsuji, K.; Yoshizawa, T. *Proc. Natl. Acad. Sci. U.S.A.* **1993**, *90*, 4072−4076.

(21) Kandori, H.; Matuoka, S.; Shichida, Y.; Yoshizawa, T.; Ito, M.; Tsukida, K.; Balogh-Nair, V.; Nakatsuji, K. *Biochemistry* **1989**, *28*, 6460−6467.

(22) Kandori, H.; Sasabe, H.; Nakatsuji, K.; Yoshizawa, T.; Mizukami, T.; Shichida, Y. *J. Am. Chem. Soc.* **1996**, *118*, 1002−1005.

(23) De Vico, L.; Page, C. S.; Garavelli, M.; Bernardi, F.; Basosi, R.; Olivucci, M. *J. Am. Chem. Soc.* **2002**, *124*, 4124−4134.

(24) De Vico, L.; Garavelli, M.; Bernardi, F.; Olivucci, M. *J. Am. Chem. Soc.* **2005**, *127*, 2433−2442.

(25) Send, R.; Sundholm, D. *J. Phys. Chem. A* **2007**, *111*, 27−33.

(26) Valsson, O.; Filippi, C. *J. Chem. Theory Comput.* **2010**, *6*, 1275−1292.

(27) Valsson, O.; Angeli, C.; Filippi, C. *Phys. Chem. Chem. Phys.* **2012**, *14*, 11015−11020.

(28) Page, C. S.; Olivucci, M. *J. Comput. Chem.* **2003**, *24*, 298−309.

(29) Gozem, S.; Huntress, M.; Schapiro, I.; Lindh, R.; Granovsky, A.; Angeli, C.; Olivucci, M. *J. Chem. Theory Comput.* **2012**, *8*, 4069−4080.

(30) Gozem, S.; Melaccio, F.; Lindh, R.; Krylov, A. I.; Granovsky, A. A.; Angeli, C.; Olivucci, M. *J. Chem. Theory Comput.* **2013**, *9*, 4495−4506.

(31) Widmark, P.; Malmqvist, P.; Roos, B. *Theor. Chem. Acc.* **1990**, *77*, 291−306.

(32) Werner, H.-J.; Knowles, P. J.; Knizia, G.; Manby, F. R.; Schütz, M.; Celani, P.; Korona, T.; Lindh, R.; Mitrushenkov, A.; Rauhut, G.; Shamasundar, K. R.; Adler, T. B.; Amos, R. D.; Bernhardsson, A.; Berning, A.; et al. *MOLPRO Quantum Chemistry Package*, version 2010.1; 2012. http://www.molpro.net.

(33) Celani, P.; Werner, H.-J. *J. Chem. Phys.* **2000**, *112*, 5546−5557.

(34) Garavelli, M.; Vreven, T.; Celani, P.; Bernardi, F.; Robb, M. A.; Olivucci, M. *J. Am. Chem. Soc.* **1998**, *120*, 1285−1288.

(35) Garavelli, M.; Negri, F.; Olivucci, M. *J. Am. Chem. Soc.* **1999**, *121*, 1023−1029.

(36) González-Luque, R.; Garavelli, M.; Bernardi, F.; Merchán, M.; Robb, M. A.; Olivucci, M. *Proc. Natl. Acad. Sci. U.S.A.* **2000**, *97*, 9379−9384.

(37) Schaftenaar, G.; Noordik, J. H. *J. Comput.-Aided Mol. Des.* **2000**, *14*, 123−134.

(38) Ghigo, G.; Roos, B. O.; Malmqvist, P.-Å. *Chem. Phys. Lett.* **2004**, *396*, 142−149.

(39) Finley, J.; Malmqvist, P.; Roos, B.; Serrano-Andrés, L. *Chem. Phys. Lett.* **1998**, *288*, 299−306.
(40) Roos, B.; Andersson, K. *Chem. Phys. Lett.* **1995**, *245*, 215−223.
(41) Kats, D.; Korona, T.; Schütz, M. *J. Chem. Phys.* **2006**, *125*, 104106.
(42) Werner, H.-J.; Manby, F. R.; Knowles, P. J. *J. Chem. Phys.* **2003**, *118*, 8149−8160.
(43) Weigend, F.; Häser, M. *Theor. Chem. Acc.* **1997**, *97*, 331.
(44) Weigend, F.; Köhn, A.; Hättig, C. *J. Chem. Phys.* **2002**, *116*, 3175−3183.
(45) *Turbomole*; a development of University of Karlsruhe and Forschungszentrum Karlsruhe GmbH, V6.4. 2012; TURBOMOLE GmbH since 2007. Available from http://www.turbomole.com.
(46) Frisch, M. J.; Trucks, G. W.; Schlegel, H. B.; Scuseria, G. E.; Robb, M. A.; Cheeseman, J. R.; Scalmani, G.; Barone, V.; Mennucci, B.; Petersson, G. A.; Nakatsuji, H.; Caricato, M.; Li, X.; Hratchian, H. P.; Izmaylov, A. F.; et al. *Gaussian 09*, Revision C.01; Gaussian Inc.: Wallingford, CT, 2011.
(47) Becke, A. *Phys. Rev. A* **1988**, *38*, 3098−3100.
(48) Lee, C.; Yang, W.; Parr, R. *Phys. Rev. B* **1988**, *37*, 785−789.
(49) Becke, A. *J. Chem. Phys.* **1993**, *98*, 5648−5652.
(50) Stephens, P.; Devlin, F.; Chabalowski, C.; Frisch, M. *J. Phys. Chem.* **1994**, *98*, 11623−11627.
(51) Yanai, T.; Tew, D.; Handy, N. *Chem. Phys. Lett.* **2004**, *393*, 51−57.
(52) Adamo, C.; Barone, V. *J. Chem. Phys.* **1999**, *110*, 6158−6169.
(53) Aquilante, F.; Vico, L. D.; Ferré, N.; Ghigo, G.; Malmqvist, P.-Å.; Neogrády, P.; Pedersen, T. B.; Pitonak, M.; Reiher, M.; Roos, B. O.; Serrano-Andrés, L.; Urban, M.; Veryazov, V.; Lindh, R. *J. Comput. Chem.* **2010**, *31*, 224.
(54) Aquino, A. J. A.; Barbatti, M.; Lischka, H. *ChemPhysChem* **2006**, *7*, 2089−2096.
(55) Wanko, M.; Hoffmann, M.; Strodel, P.; Koslowski, A.; Thiel, W.; Neese, F.; Frauenheim, T.; Elstner, M. *J. Phys. Chem. A* **2005**, *109*, 3606−3615.
(56) Hufen, J.; Sugihara, M.; Buss, V. *J. Phys. Chem. B* **2004**, *108*, 20419−20426.
(57) Cembran, A.; González-Luque, R.; Altoè, P.; Merchán, M.; Bernardi, F.; Olivucci, M.; Garavelli, M. *J. Phys. Chem. A* **2005**, *109*, 6597−6605.
(58) Valsson, O.; Campomanes, P.; Tavernelli, I.; Rothlisberger, U.; Filippi, C. *J. Chem. Theory Comput.* **2013**, *9*, 2441−2454.
(59) Huix-Rotllant, M.; Filatov, M.; Gozem, S.; Schapiro, I.; Olivucci, M.; Ferré, N. *J. Chem. Theory Comput.* **2013**, *9*, 3917−3932.
(60) Szalay, P. G.; Watson, T.; Perera, A.; Lotrich, V. F.; Bartlett, R. J. *J. Phys. Chem. A* **2012**, *116*, 6702−6710.
(61) Silva-Junior, M. R.; Schreiber, M.; Sauer, S. P. A.; Thiel, W. *J. Chem. Phys.* **2008**, *129*, 104103.
(62) Schreiber, M.; Silva-Junior, M. R.; Sauer, S. P. A.; Thiel, W. *J. Chem. Phys.* **2008**, *128*, 134110.
(63) Caricato, M.; Trucks, G. W.; Frisch, M. J.; Wiberg, K. B. *J. Chem. Theory Comput.* **2011**, *7*, 456−466.